Taylor & Francis
Taylor & Francis Group

Computer Methods in Biomechanics and Biomedical Engineering

ISSN: 1025-5842 (Print) 1476-8259 (Online) Journal homepage: http://www.tandfonline.com/loi/gcmb20

Computational investigations on the hemodynamic performance of a new swirl generator in bifurcated arteries

B. Prashantha & S. Anish

To cite this article: B. Prashantha & S. Anish (2019): Computational investigations on the hemodynamic performance of a new swirl generator in bifurcated arteries, Computer Methods in Biomechanics and Biomedical Engineering, DOI: 10.1080/10255842.2018.1556974

To link to this article: https://doi.org/10.1080/10255842.2018.1556974

Published online: 20 Jan 2019.

COMPUTER METHODS IN BIOMECHANICS AND BIOMEDICAL ENGINEERING
https://doi.org/10.1080/10255842.2018.1556974

Computational investigations on the hemodynamic performance of a new swirl generator in bifurcated arteries

B. Prashantha[a] and S. Anish[b]

[a]Department of Mechanical Engineering, M S Ramaiah Institute of Technology, Bengaluru, Karnataka, India; [b]Advanced Fluid Mechanics Laboratory, Department of Mechanical Engineering, National Institute of Technology, Surathkal, Karnataka, India

ABSTRACT

Hemodynamic behaviour of blood in the bifurcated arteries are closely related to the development of cardiovascular disease. The secondary flows generated at the bifurcation zone promotes the deposition of atherogenic particles on the outer walls. The present study aims at suppressing the development of atherosclerosis plaque by inducing helical flow structure in the arterial passage. To realize this objective a novel swirl generator (stent like structure with an internal groove) has been developed to induce helicity in the bifurcated passage. The functional requirement of the swirl generator is to minimize the relative residence time (RRT) of the fluid layer near the endothelial wall without generating any additional pressure drop. Different configurations of the swirl generator have been tested computationally using large eddy simulation (LES) model. It is observed that the induced helical flow redistributes the kinetic energy from the centre to the periphery. A single rib swirl flow generator proximal to the stent treated passage can generate sufficient helicity to bring down the RRT by 36% without generating any additional pressure drop. The swirl flow adds azimuthal instability which increase vortex formations in the passage. The induced helical flow in the domain provokes more linked vortices, which may act as self-cleaning mechanism to the arterial wall.

ARTICLE HISTORY
Received 25 July 2018
Accepted 1 December 2018

KEYWORDS
Bifurcated artery; hemodynamics; swirl flow generator; relative residence time; helicity

1. Introduction

Cardiovascular disease (CVD) is the leading cause of death worldwide (WHO 2016). Hemodynamic characteristics in an arterial blood vessel are closely related to the development of CVDs. The initial step towards the progression of atherosclerosis plaque involves the accumulation of low density lipoproteins (LDL) and macrophages in the endothelium layer. Quite often, local recirculation of blood flow near the curved region or branched region can lead to plaque formation (Prashantha and Anish 2018). Incidentally, the relative residence time of the fluid layer near these locations may be quite high, which enhance the probability of settling of atherogenic particles in these locations (Zovatto and Pedrizzetti 2017). High value of the Relative Residence Time (RRT), which indicates the time of residence the molecules spent at endothelium, have been emerging as appropriate tools for identifying the possible regions of atheromatic plaque localization (Himburg et al. 2004, Soulis et al. 2011).

Several studies have reported the presence of swirl flow in the human circulatory system (Houston et al. 2004, Morbiducci et al. 2011, Stonebridge and Brophy 1991). Inherently the blood flow through artery is spiral type because of the twisting of heart on its own axis (Stonebridge and Brophy 1991, Stonebridge et al. 2004). Apart from this, the physiological states and certain combination of pulsatile flow through the non-planarity of arterial wall may induce additional swirl/helical flow pattern in the vessel (Basavaraja et al. 2017, Caro et al. 1996, Gallo et al. 2012). The spiral component of blood velocity can have both beneficial and detrimental effects according to Stonebridge and Brophy (1991). The swirl flow supresses the localization of low density lipoproteins (LDL) and accelerates mass transport in the lumen vessel (Chen et al. 2017, Gataulin et al. 2015, Ha et al. 2015, Liu et al. 2015, Stonebridge et al. 2004, Sun et al. 2010, Wong et al. 2010, Zovatto and Pedrizzetti 2017). On the other hand, spiral flow may reduce the recirculation flow region length and results in an early breakout of transition to turbulence (Gataulin et al. 2015, Ha et al. 2015, Ha et al. 2014, Ha and Lee 2013, Ha and Lee 2014). At low Reynolds number the

CONTACT S. Anish anish@nitk.edu.in Advanced Fluid Mechanics Laboratory, Department of Mechanical Engineering, National Institute of Technology, Surathkal, Karnataka, India

turbulent kinetic energy is reduced by the spiral flow as it induces the rotational stabilities in the forward flow. However, at higher Reynolds number (Re = 1000) no significant difference is found in the centreline turbulent kinetic energy between the spiral and non-spiral flows and the effect is mild on the centreline shear stresses (Paul and Larman 2009).

Several efforts have been made elsewhere to induce the spiral flow artificially in the arteries. Much of the studies were in the use of vascular graft. To increase cross-plane mixing of the fluid, Caro et al. (2005) developed a helical-shaped vascular graft that generates swirling flow. Van Canneyt et al. (2013) and Wen et al. (2011) simulated the hemodynamic characteristics of several arteriovenous grafts with various helical shapes. Zeller et al. (2016) and Sullivan et al. (2018) developed 'BioMimics' 3 D helical stent to induce laminar swirling blood flow and elevate vascular wall shear in the treated segment. The BioMimics 3 D stent, promotes an increase in swirling blood flow and wall shear, may have patency benefits when compared with a straight stent.

The objective of the present work, is to develop an alternate method to induce helicity in the carotid bifurcation arteries in order to reduce the relative residence time in the recirculation zone. We propose the use of swirl generator, stent like device with an internal grooves, which can induce helicity to the arterial flow. We aim for the conceptual design of swirl generator from the hemodynamic perspective in an idealized bifurcated passage. Several designs have been tested to minimize the relative residence time near the bifurcation zone, while keeping the induced flow resistance to a minimum.

2. Methods

2.1. The computational model

Present numerical study has been carried out on a population-based healthy idealized bifurcated geometry similar to the carotid artery. Such an idealized model-based approach will enable to carry out a more rigorous systematic study, by varying one specific geometrical feature at a time while keeping the others constant. This enables to identify if and to which extent anatomic features promote atheroprotective or atherosusceptible hemodynamic phenotypes (Chiastra et al. 2017). The vessel geometry and the diameter ratio specifications were taken from the works by Ku et al. (1985) and Schulz and Rothwell (2001).

Blood is modelled as Newtonian fluid with density and dynamic viscosity as 1060 kg/m^3 and 0.0036014 $Pa\,s$ respectively (Banks and Bressloff 2007, Mukherjee et al. 2016). The simulations are carried out with FLUENT. The inflow velocity profile used for the present simulation is taken from the profiles used by Hoi et al. (2010) and Gataulin et al. (2015) in their studies. At the outlet constant pressure boundary condition is specified. The boundary wall is assumed to be rigid and no slip condition is specified (Balossino et al. 2009, Lee and Steinman 2007, Linge et al. 2014, Morbiducci et al. 2011). To achieve converged solution for each time step, inner loop has been set to 30 with a time step size of 0.0001 s. The inner loop refers the number of iterations to be carried out in each time step. The turbulence methodology adopted for this study is the Large Eddy Simulation (LES). LES resolves the larger turbulent eddies whereas the smaller ones are modelled during the pulsatile flow (Lantz et al. 2016, Varghese et al. 2008). The classic Smagorinsky LES model is closer to DNS data (Varghese et al. 2007). Hence the present simulation has been carried out with LES Samgorinsky model. Very fine grids have been generated to each geometric model so that the maximum value for y + can be maintained smaller than 1 (Figure 1). The computations are performed on a windows 64 bit operating system with Dual processor (2 no.) INTEL XEON V3 8cores, 64GB RAM.

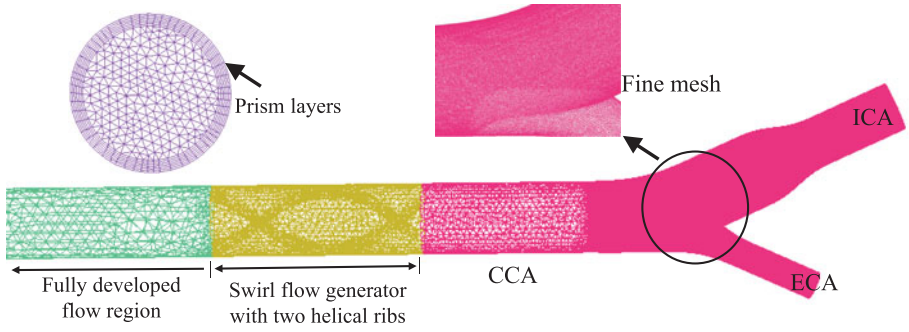

Figure 1. Computational grid used for the simulation showing swirl generator with two helical ribs.

2.2. The swirl generator

The present study numerically tests the conceptual design of a new device, the swirl generator that generate helical flow structure in the bifurcated arteries. The swirl generator may be assumed as a stent like structure with an internal grooves. With these criteria, the grooves are provided with triangular ribs at the inner wall of the swirl generator. Figure 2(a) shows the idealized carotid artery model, chosen for the computational study. The common carotid artery (CCA) empties into a smaller external carotid artery (ECA) and a large internal carotid artery (ICA). The length of the helicity generator is three times the CCA diameter and it is placed five diameter proximal (-5D) to the bifurcation zone (Figure 2a) in the CCA passage. The parameters taken for analysis are height of the rib, the helical angle and the number of ribs. Each of these parameters are varied systematically to understand their influence on the hemodynamics and the atherogenises. A total number of 11 different cases are analysed whose details are shown in Figure 3 as well as in Table 1.

2.3. Validation of the numerical scheme

Validation is one of the essential step in simulation work. Present study has been validated with Ahmed and Giddens (1984) transient experimental data and shown in Figure 4. Comparisons are made for the radial variation of axial velocity during systolic peak time step at different planes. The normalized axial velocity (normalisation is done with respect to average velocity) along X-axis and normalized radial distance along Y-axis are plotted. Similar comparisons are made at different axial positons (1 D, 1.5 D, 2.5 D, 4 D & 6D). Tan et al. (2008) carried out numerical simulations on the same base model using RANS method. Present study has predicted the numerical results more accurately than other RANS based CFD studies both qualitatively and quantitatively.

2.4. Analysis of results

2.4.1. Relative residence time (RRT)

Spatial variation of wall shear stress (WSS) in the flow are derived from the velocity vectors. These vectors starts to oscillate with the unsteady flow and it changes the direction at low wall shear stress regions. Himburg et al. (2004) has suggested the use of Relative Residence Time (RRT) with the correlation of OSI and Time Averaged Wall Shear Stress (TAWSS) and is defined as

$$RRT = \frac{1}{(1 - 2{*}OSI)TAWSS} \tag{1}$$

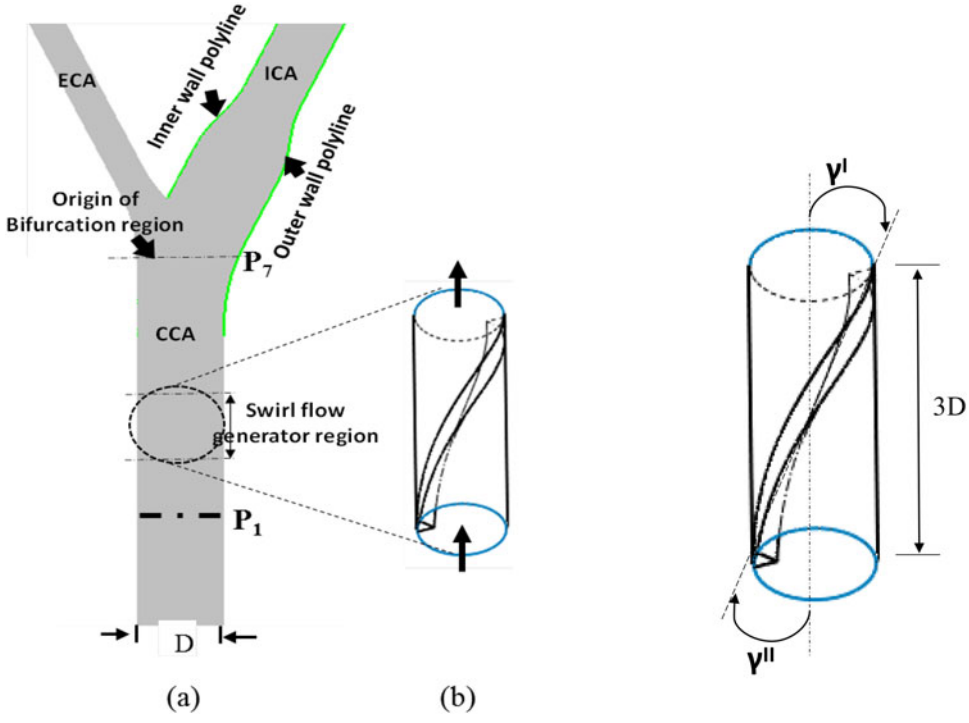

Figure 2. (a) Location of the swirl generator in the arterial passage (b) conceptual design of swirl generator (single rib), where 'γ' ($\gamma^{I}+\gamma^{II}$) is helical angle.

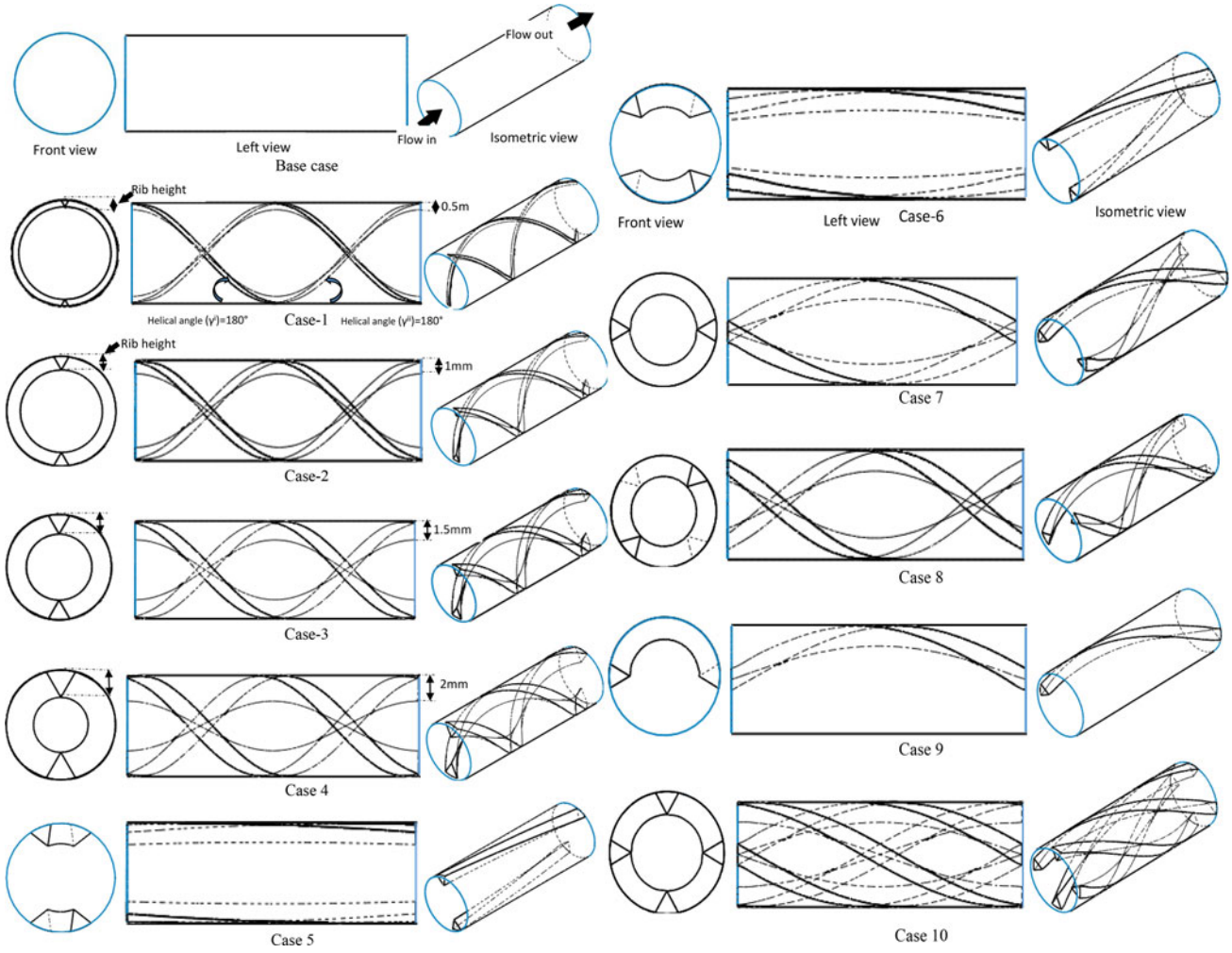

Figure 3. Schematic diagram of ten swirl flow generator designs. For comparison purpose base case is also added.

Table 1. Details of different swirl generator configuration tested and their comparative performance with base case.

Models	Rib height (mm)	Helical angle(degree)	No. of helical Ribs in the flow domain	Time average pressure difference (Pa)	Pressure drop, % deviation compared with Base case	Average Relative Residence Time (Pa^{-1})	RRT, % difference compared with Base case	Helicity intensity (h_2)
Base case	–	–	–	53.1	–	13.9	–	126.1
Case-1	0.5	360	2	57.5	8.29	10.9	21.58	176.6
Case-2	1	360	2	77.1	41.74	9.1	34.53	231.2
Case-3	1.5	360	2	110.5	74.45	4.7	66.19	294.0
Case-4	2	360	2	136.8	75.75	7.2	48.20	360.0
Case-5	1.5	45	2	66.2	9.58	11.3	18.71	167.0
Case-6	1.5	90	2	68.8	23.72	7.8	43.88	177.9
Case-7	1.5	180	2	72.2	27.76	4.8	65.47	214.5
Case-8	1.5	270	2	92.3	54.29	6.5	53.24	259.1
Case-9	1.5	180	1	53.48	0.41	8.9	35.97	191.5
Case-10	1.5	180	4	94.1	75.53	8.0	42.45	254.9

$$OSI = 0.5\left[1 - \frac{\int_0^T \overrightarrow{WSS}}{\int_0^T \overrightarrow{wss}}\right] \quad (2)$$

$$TAWSS = \frac{1}{T}\int_0^T \overrightarrow{WSS} \quad (3)$$

where T is the pulse period, $\overrightarrow{WSS}$ is the instantaneous wall shear stress. RRT indicates the residence time of fluid layer at endothelium layer of wall (Himburg et al. 2004, Soulis et al. 2011). Flow visualisation studies carried out by Ku and Giddens (1983) showed the attachment of bubbles near to the outer wall of sinus for a longer period of time, which enhances the fluid

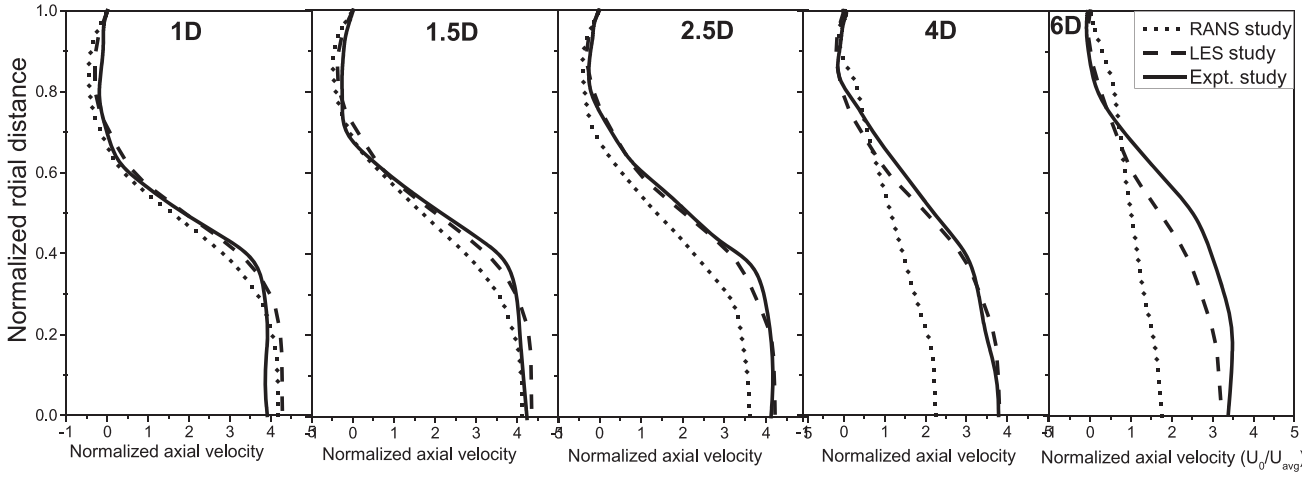

Figure 4. Comparison of normalized axial velocity along the axial direction at peak systolic time step.

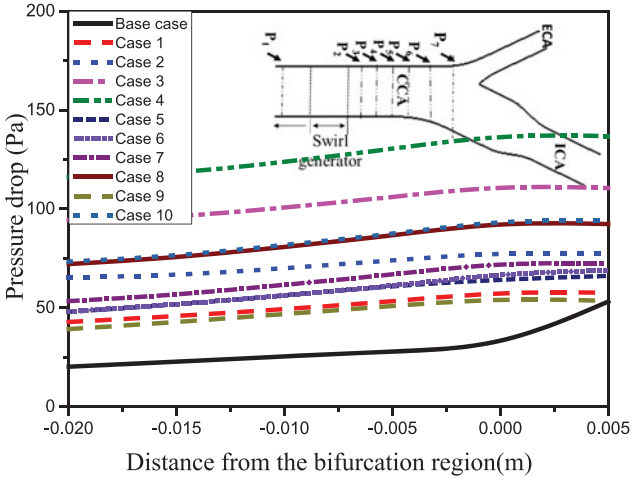

Figure 5. Variation of pressure drop from plane-2 (P2) to plane-7 (P7) along the flow direction for all swirl generator configurations. Pressure drop at location is calculated with respect to the cross sectional plane-1 (P1).

residence time. Hence, RRT can be used as an effective marker for indicting the probability of plaque formation through settlement of atherogenic materials.

2.4.2. Pressure loss in the bifurcated region

Static pressure drop in the artery is one of the most important parameter considered in the present study. An increase in the pressure drop indicates an increased flow resistance in the channel. For the comparison of flow resistance offered by different swirl generator configurations static pressure drop is calculated as the area average pressure difference between the inlet of swirl generator (P_1) and at the bifurcation section (P_7) (Figure 2). The values thus obtained are then time averaged over the entire cycle. An ideal swirl generator may be causing minimum time averaged static pressure drop.

2.4.3. Descriptors for swirl flow topology

Topology of helical flow structure in the bifurcated artery has been analysed with swirl flow strength and relative rotational direction. Following expressions are derived from Gallo et al. (2012).

$$h_1 = \frac{1}{T\ V}\int_T\int_V H\ dv\ dt \tag{4}$$

$$h_2 = \frac{1}{T\ V}\int_T\int_V |H|\ dv\ dt \tag{5}$$

$$h_3 = \frac{h_1}{h_2} \tag{6}$$

where 'T' is the cardiac pulse cycle, 'V' is the volume of fluid in domain, 'H' is the helicity and it can be expressed as $H = u.\omega$. Where 'U' is the velocity and 'ω' is the vorticity of the fluid. To define the bulk flow parameter integration is carried out over time (T) and volume (V).

The term h_1 is helical intensity, which is integral measure of helical flow accounting for helicity sign changes. h_1 equals '0' when there is no helical flow in the domain or it may have reflectional symmetric counter rotating helical structures. The parameter h_2 defines total amount of helical flow in the fluid domain, irrespective of direction. The term h_3 is a non-dimensional quantity ranging between -1 to +1. h_3 value equals -1 (+1) only when left-handed (right-handed) helical flow structures are present in the domain and it equals 0 in case of reflectional symmetry or no helical structures in the flow field.

3. Results

The swirl generator must provide enough helicity to minimize the relative residence time of the fluid layer closer to the wall and at the same time it should not be creating significant pressure drop and additional fluid resistance in the arterial passage. Hence, the results are analysed based on the helicity induced, the relative residence time (RRT) and the pressure drop in the passage.

3.1. Effect of swirl generator on the hemodynamics

The relative residence time at the bifurcation zone, time averaged pressure drop across the CCA and the helicity descriptor h_2 are calculated for all the designs. Table 1 gives a comprehensive view for all these parameters for each design as well as their percentage deviation compared to the base case. As the objective of this swirl generator is to reduce the *RRT* near the bifurcated channels, design with least *RRT* (i.e. Case 3) might have been the best selection. However, it causes a pressure drop of 110.5 Pa which is 107% more than the base case. The swirl generator must create minimum blockage and flow resistance to the flow while minimizing the RRT. Owing to this condition, Case 9 stands out as the best choice as it does not generate any additional pressure drop compared to the base case, while bringing down the RRT by 36%.

Figure 5 shows the static pressure drop variation for all the swirl generator configurations. For the ease of analysis, area averaged static pressure values are noted at seven cross sectional planes. These planes are named as P_1, P_2, P_3, P_4, P_5, P_6 and P_7 respectively. The pressure drop values at each location is calculated with respect to plane-1 (P_1) and the values are plotted from plane-2 (P_2) to plane-7 (P_7). The location of these cross sectional planes with respect to bifurcation region is shown in the *X* axis of Figure 5. Plane-6 corresponds to the beginning of the bifurcation region. The pressure drop values are steadily increasing for all the configurations; however, the least pressure drop occurs with Case 9. A rapid pressure drop is observed for base case at the bifurcation region, possibly due to the flow separation at that region. The flow separation is weakened by the induced helicity by the swirl generator.

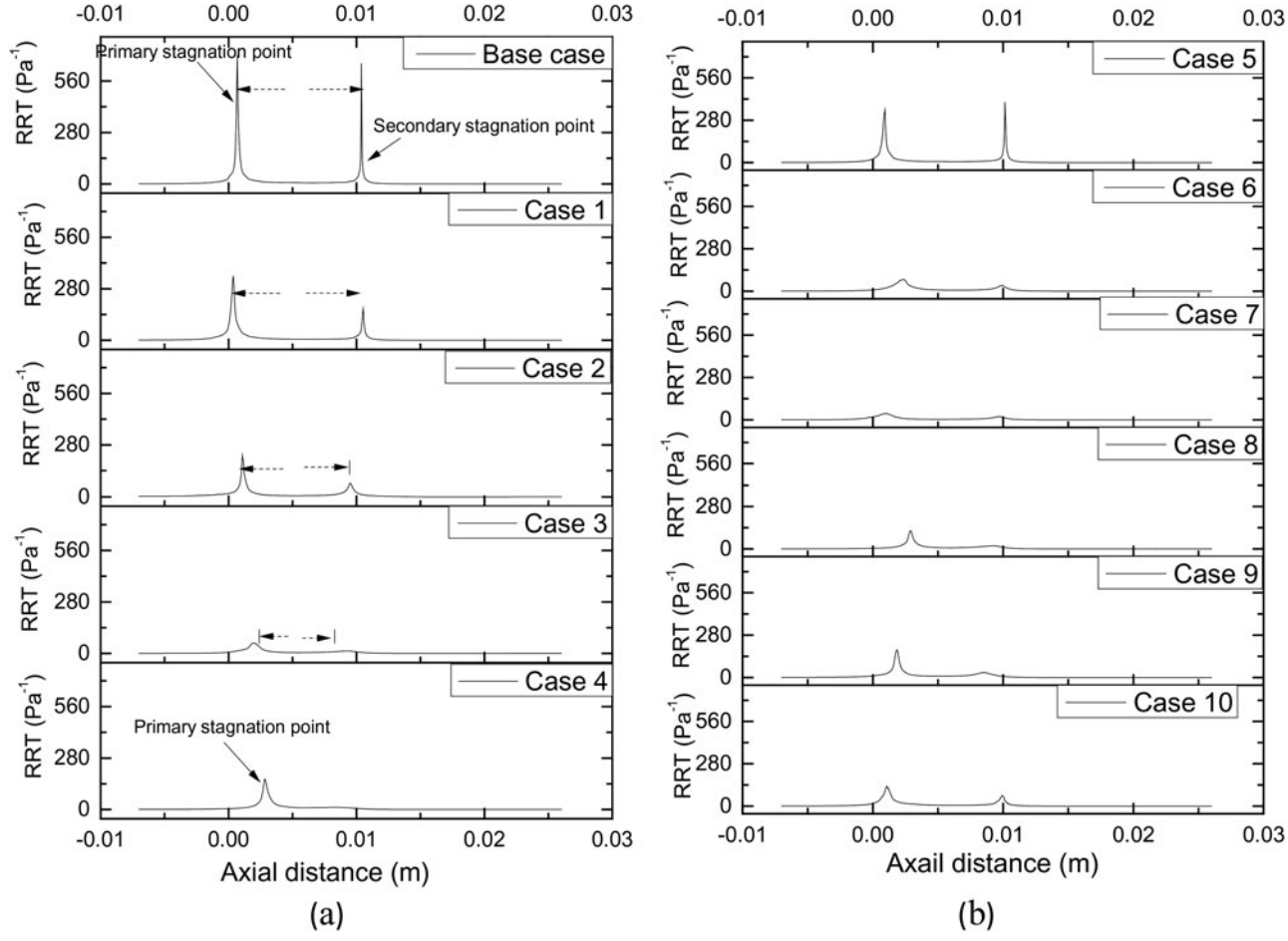

Figure 6. Relative residence time of fluid layers near the ICA outer wall compared with Base case.

3.2. Relative residence time (RRT) analysis

Figure 6 shows the relative residence time of ten swirl generator designs in comparison with the base case. The RRT has been plotted on the outer wall of the ICA as major separated region are centred here. The two peaks observed in the RRT plots, correspond to two stagnation points formed within the recirculation regions. The introduction of swirl generator reduces RRT of each design at varying magnitude. The effect of rib height on RRT is visible from the comparison of Cases 1 – 4. With increase in the rib height the two stagnation points comes closer and with a rib height of 2 mm the second stagnation point almost disappears (Case 4).

Cases 5 – 8 depicts the variation of RRT with the helical angle of the rib. A large helical angle induces more helicity to the flow. However, the RRT values need not be always come down with increased helicity. This is evident with the comparison between Case 7 and Case 8. With an increase in helical angle from γ =180 deg. (Case 7) to γ = 270 deg. (Case 8) the helicity induced increases by 20% but the RRT value also increases from 4.8 to 6.5. The residence time again comes down to 4.7 when the helical angle is increased to 360 deg. (Case 3). The reasons for this unforeseen behaviour may be explained with helicity contours plotted at two cross sections near the bifurcation zone (Figure 7). These are instantaneous values of helicity plotted at deceleration time step. For a helical angle of 270 deg. the flow streamlines gets modified in such a way that the helicity contours (both clockwise spin and anticlockwise spin) are moved away from the outer wall of the ICA. The outer wall of the ICA is seen mostly with zero helicity and is characterized by strong local recirculation and low wall shear stress (WSS) which will enhance the residence time of fluid near the wall (Arzani et al. 2017, Jiménez and Davies 2009). This implies that even though the volumetric average of helicity (h_2) increases with helical angle the same may not reflect in the RRT which is basically a function of the local values of helicity.

The number of ribs is an another important parameter which can influence the helicity generated and the RRT. A helical angle of 180 deg. and a rib height of 1.5 mm is selected as the optimum choice based on the smaller relative residence time. Hence fixing these configurations the number of ribs are varied and the simulations are carried out. Comparing the Cases 7, 9 and 10 it turns out that, single rib configuration produce least flow resistance. The pressure drop generated by Case 9 is similar to that of base case while reducing the RRT by 36%. Increase in the rib height from 1.5 mm to 2 mm enhance the turbulence which results in more resistance to the fluid flow. As a result, the pressure drop increases roughly by 24% with a small increment of rib height.

3.3. Detailed analysis on the flow modifications

Velocity contours at the central axial plane has been plotted and shown in Figure 8. The primary and secondary stagnation point which are responsible for two peaks in the RRT plot has been demarcated in this figure. As a result of the helical movement, the kinetic energy has been redistributed from the centre of the arterial passage to the periphery. This helps in mitigating the recirculation regions near the bifurcation passage. As the rib height increases it induces more helicity and the primary stagnation point moves distal to the bifurcation region. The effective flow area also

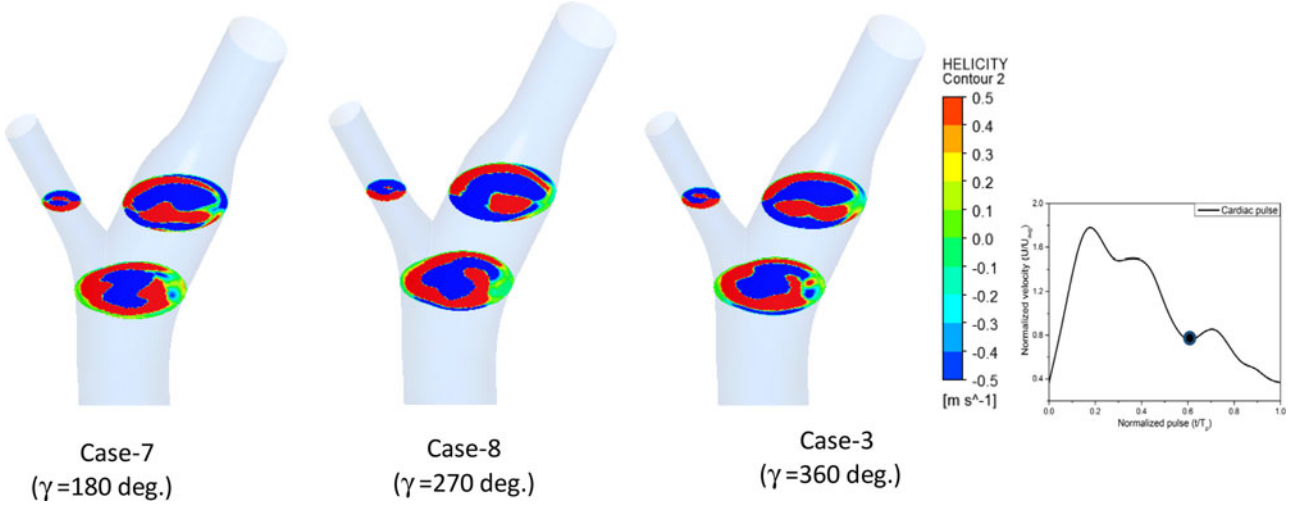

Figure 7. Helicity contours for different helical angles at the bifurcation region during diastolic deceleration time step.

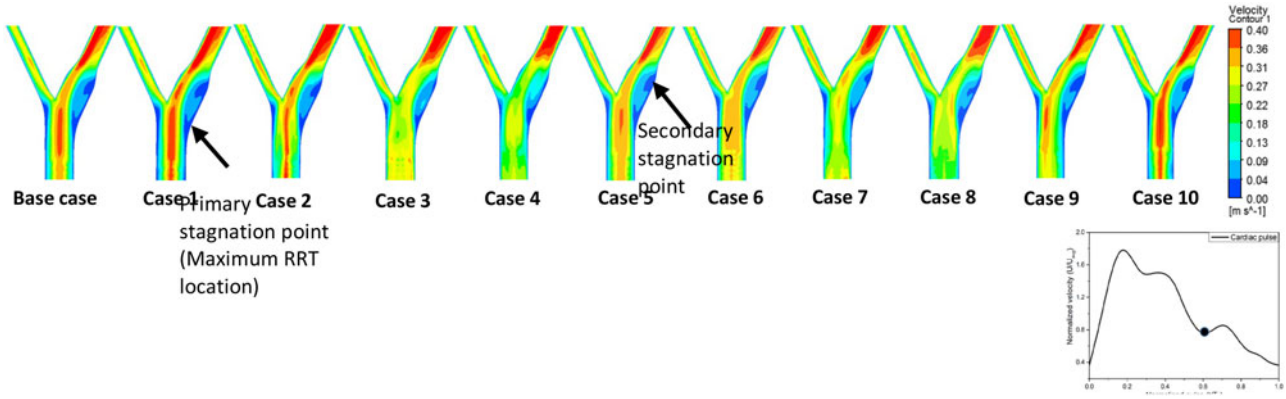

Figure 8. Velocity contours at an axial plane during deceleration time step.

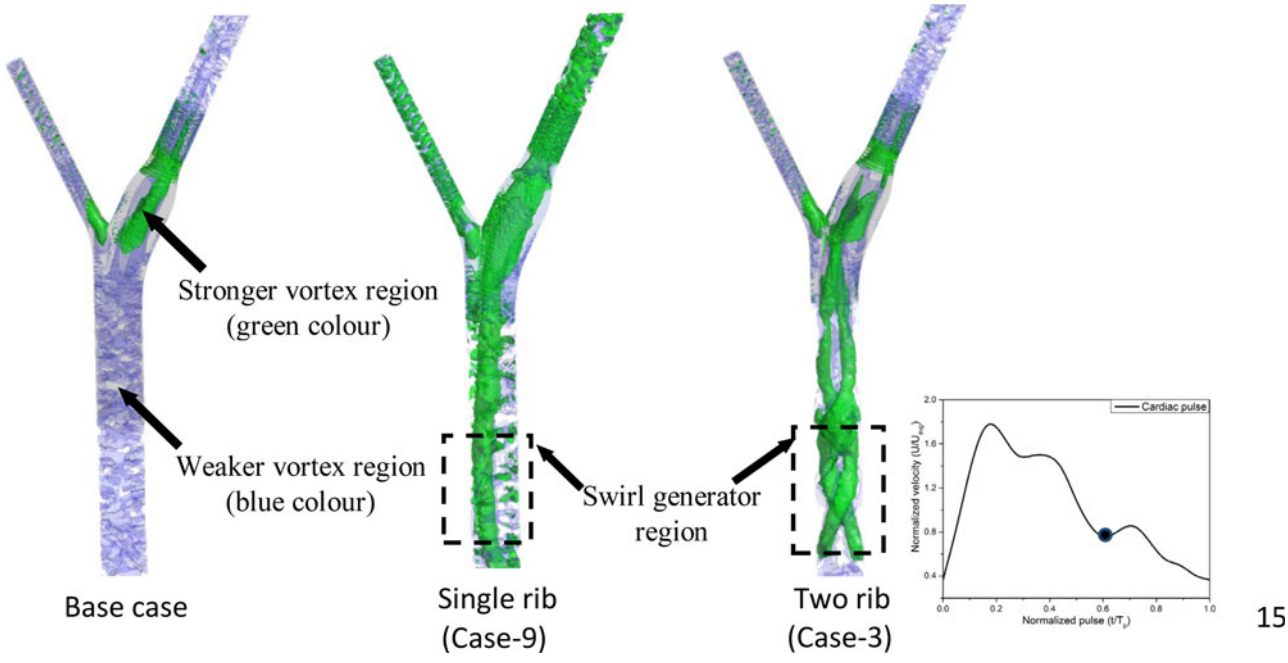

Figure 9. Coherent vortical structures expressed with Q criterion during diastolic instance.(a).

increases in the sinus region due to the increased helicity.

Presence of coherent vortical structures in the flow field are identified by Q-criterion (Hunt and Hussain 1991) and shown in Figure 9. The vortical structures are drawn at diastolic deceleration time instance for two different isovalues. The comparison is made with base case, single rib (Case 9) and two rib (Case 3) configurations. Smaller, weak vortices are filled in the CCA for the base case. These weaker vortices are washed away by a strong linked vortex in single rib design and two strong swirling vortices in the case of two rib configuration. The vortices present in the sinus region of base case is formed mainly due to the bifurcation. They are seen at the middle of the passage without getting connected to the recirculation zone. Absence of swirl velocity component enhances more rigid vortices in the sinus region (Kolář 2007). It provokes the atherogenic particles to settle on the arterial wall. During the cardiac cycle, swirl generator induces strong swirl velocity component which intersect with weaker vortices at the sinus region. Random movement of weaker vortices is restricted by the action of swirl flow which washes out the weaker vortices component. Existence of stronger shear layers can be observed in the flow domain. Hence, in the swirl generator case sinus region gets filled with helical flows which are instrumental in reducing the stagnant regions.

With increasing rib height, helical angle and number of ribs the swirl generator induces more helicity in the arterial passage. Basically two counter rotating helical flow structures are generated in the passage. One with negative helicity (clockwise spin) in the ICA and with positive helicity (anticlockwise spin) in the ECA. A helical flow which replicates lower

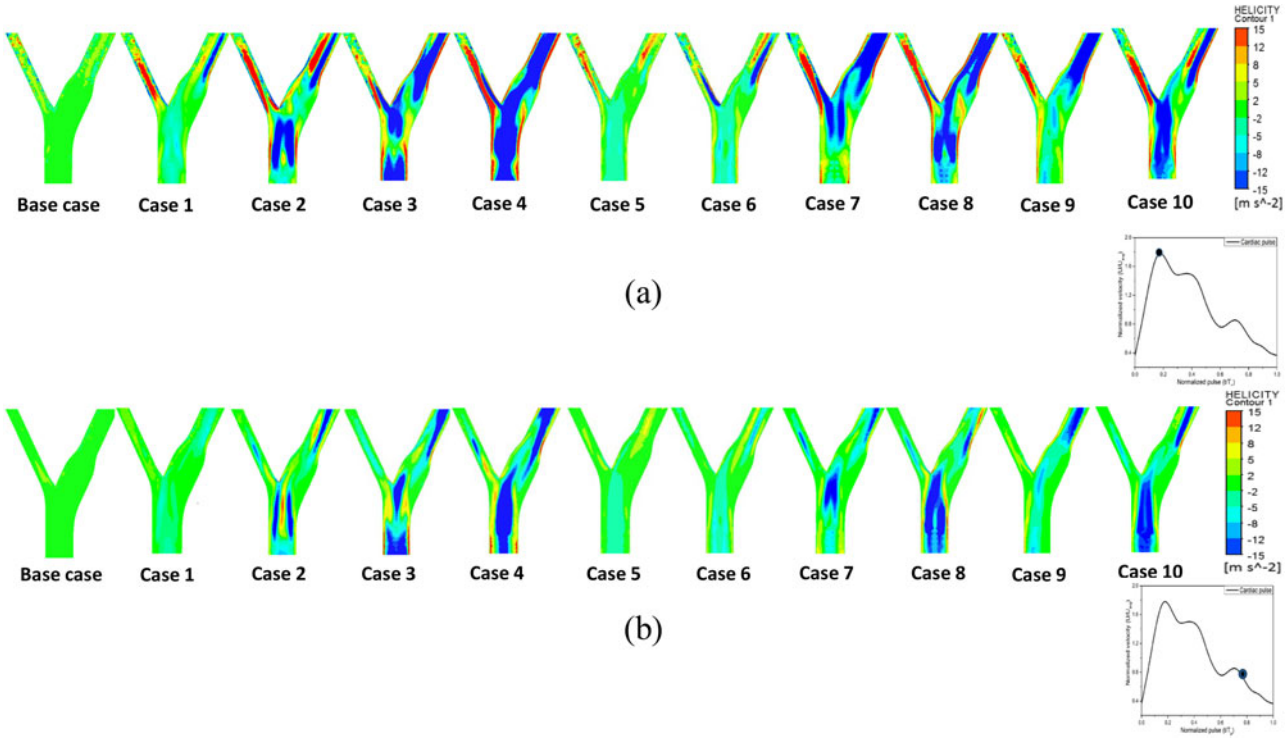

Figure 10. Helicity contours (a) Peak systolic (b) Diastolic deceleration time step.

residence time with moderate pressure drop has favourable hemodynamic in the artery.

Figure 10 represents the helicity induced at peak systolic as well as diastolic instances. The base case is devoid of any helicity mostly during the diastolic instance. Alignment of helix in the swirl generator induces anticlockwise spin near the periphery and clockwise spin at the centre. Strengthened clockwise vortex at the centre pushes the weakened vortices surrounding it to the arterial wall (Lee et al. 2011). This is evident from the plot of helical descriptors h_3 (Figure 11). The value of h_3 vary from -1 to +1. Results indicate that base case inherently has a small positive spin while the swirl generator induces mainly a clockwise spin (negative vorticity) to the fluid domain.

4. Discussions

The degenerative material responsible for atherosclerotic plaque settles mainly at the outer ICA sinus region of the bifurcation zone (Berger and Jou 2000, Chiastra et al. 2017, Huang et al. 2014, Perktold et al. 1991, Pinto and Campos 2016, Steinman et al. 2000). Maximum relative residence time appears at this location and two stagnation points are observed. The primary stagnation point appears due to the separation of the boundary layer from the outer wall of the ICA, whereas the secondary one appears at the point of reattachment. Inside the boundary layer flow reversal happens whose starting and ending points are demarcated by these two stagnation points. The helical flow makes the maximum kinetic energy from the centre to redistribute to the periphery. Due to this outward bound energy transfer from the central region, the boundary layer fluid gets energized. This delays the separation and hence the primary stagnation point move distal to the bifurcation region.

Helical or swirl flow can minimize the risk factors that causes the atherogenesis. It can suppress the low and oscillating shear and act as a protective mechanism against plaque formation (Gataulin et al. 2015, Ha et al. 2015, Liu et al. 2015, Morbiducci et al. 2009, Stonebridge et al. 2004, Sun et al. 2010, Wong et al. 2010, Zheng et al. 2014, Zovatto and Pedrizzetti 2017). The present study reveals that adding a single rib swirl flow generator proximal to the stent treated passage can generate sufficient helicity to bring down the RRT 36% without creating any flow disturbances. The helicity values are positive near the wall, possibly due to the large velocity gradient in the radial direction. Predominantly negative helicity is induced in the main passage. However, after the bifurcation, both helicity streams (with opposite spin) interact in the sinus region. If the recirculation regions are pulled inside the helicity contours, then the RRT comes down as seen in Case 3. On the other hand, an improper helical angle makes the helical core regions

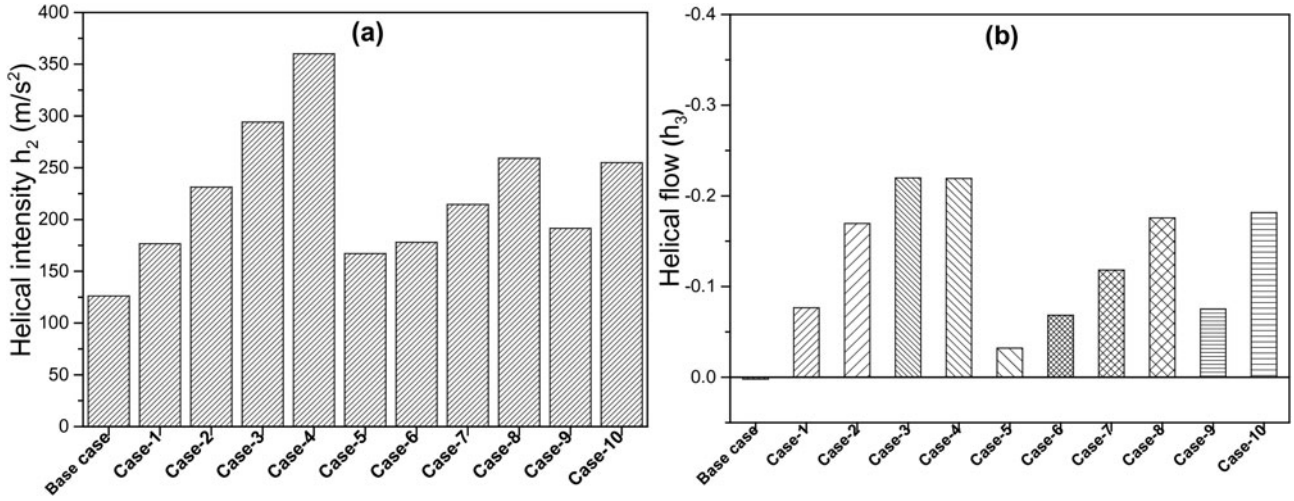

Figure 11. Quantitative analysis of helical flow strength in the bifurcated artery (a) Amount of helical flow in the domain represented with helical intensity (b) Helical flow structures in the domain.

move away from the recirculation zone. Under such circumstances the RRT value may be still high even though a large helicity is induced in the passage (as observed with Case 8).

Absence of swirl flow in the arteries makes it a poiseuille flow which may generate Kelvin–Helmholtz instability between centreline velocity of stream and surrounding fluid near to the wall region (Ha et al. 2015). The swirl flow adds azimuthal instability which increase vortex formations in the passage. Increased vortex formation enhances the mass, energy and momentum transport near to the wall region (Caro et al. 2013, Ha et al. 2015, Liang and Maxworthy 2005, Ma et al. 1997). Kilner et al. (1993) observed corkscrew like flow pattern in the ascending aorta as a result no atherosclerotic plaque formation occurs in this region. This vortex formation is different from the vortices formed at the separated recirculation regions and the bifurcated zones. The induced helical flow in the domain provokes more linked vortices (coherent vortices), which may act as self-cleaning the arterial wall. If the helical angle is not oriented properly the induced vortices may not efficiently bring down the residence time. In such cases, larger helical flow may not be very useful to prevent atherogenises.

A high value of helicity in the flow structure can increase in the flow resistance. The pressure drop incurred in the passage can be a measure of this flow resistance. The selection of the swirl generator has to be made based on the minimum time averaged pressure drop occurred in the passage. Among ten swirl case generator that has been tested Case-9 has been suggested for clinical practice as it does not offer any additional pressure drop, but reduces the RRT by 36%.

5. Conclusions

A computational investigation has been carried out on an idealized bifurcated artery to understand the effect of an induced helicity on the hemodynamics. For inducing helicity, a swirl generator has been proposed. The present study focuses on the conceptual design of the swirl generator and it is looks as a stent-like device with an internal grove. It is observed that generation of helical flow and disturbed shear layers in the complex flow field is effectively suppressing the recirculation zones. Thus the, accumulation of atherogenic particles is minimized by controlling the relative residence time of fluid layer near the wall. The height of the rib, helical angle and number of rib have varied systematically to identify an ideal swirl generator which brings down the RRT while offering minimum flow resistance. Two stagnant regions are observed at the outer wall of the ICA. With increased helicity the primary stagnation point moves distal to the bifurcation region. The helical flow makes redistribution of the kinetic energy from the centre to the periphery. This outward bound energy transfer from the central region, makes the boundary layer fluid gets energized causing a delay in the separation of fluid layer from the arterial wall. Among the tested configurations, swirl generator with single rib and 180 deg. helical angle offers 36% reduction in the relative residence time without creating any significant flow resistance. Detailed flow analysis revealed the existence of stronger shear layers due to the induced helicity which washes out the weaker vortices component by the action of swirl flow. This mechanism enhances the wash out of atherogenic particles at the bifurcation zone, thereby minimizing the chances of atherosclerosis.

The present study has the following limitations. Only conceptual design of the swirl generator has been made and subsequent effect on the hemodynamics alone is considered in this study. Computational simulations are carried out on an idealized bifurcated artery. The induced helicity pattern may be different in a real corrugxated artery. The walls are assumed to be rigid and hence the fluid structure interactions effects have not been considered.

Declaration

There are no competing interests and no funding agency is involved in the study. Ethical approval is not required as the studies were carried out on an idealized artery.

References

Ahmed SA, Giddens DP. 1984. Pulsatile poststenotic flow studies with laser Doppler anemometry. J Biomech. 17(9):695–705.

Arzani A, Gambaruto AM, Chen G, Shadden SC. 2017. Wall shear stress exposure time: a Lagrangian measure of near-wall stagnation and concentration in cardiovascular flows. Biomech Model Mechanobiol. 16(3):787–803.

Balossino R, Pennati G, Migliavacca F, Formaggia L, Veneziani A, Tuveri M, Dubini G. 2009. Influence of boundary conditions on fluid dynamics in models of the cardiovascular system: a multiscale approach applied to the carotid bifurcation. Comput Meth Biomech Biomed Eng. 12:1–13.

Banks J, Bressloff N. 2007. Turbulence modeling in three-dimensional stenosed arterial bifurcations. J Biomech Eng. 129(1):40–50.

Basavaraja P, Surendran A, Gupta A, Saba L, Laird JR, Nicolaides A, Mtui EE, Baradaran H, Lavra F, Suri JS. 2017. Wall shear stress and oscillatory shear index distribution in carotid artery with varying degree of stenosis: a hemodynamic study. J Mech Med Biol. 17(02):1750037.

Berger S, Jou L-D. 2000. Flows in stenotic vessels. Annu Rev Fluid Mech. 32(1):347–382.

Caro CG, Cheshire NJ, Watkins N. 2005. Preliminary comparative study of small amplitude helical and conventional ePTFE arteriovenous shunts in pigs. J Royal Soc Interface. 2(3):261–266.

Caro CG, Doorly DJ, Tarnawski M, Scott KT, Long Q, Dumoulin CL. 1996. Non-planar curvature and branching of arteries and non-planar-type flow. Proc R Soc Lond A. 452(1944):185–197.

Caro CG, Seneviratne A, Heraty KB, Monaco C, Burke MG, Krams R, Chang CC, Coppola G, Gilson P. 2013. Intimal hyperplasia following implantation of helical-centreline and straight-centreline stents in common carotid arteries in healthy pigs: influence of intraluminal flow. J Royal Soc Interface. 10(89):20130578.

Chen WX, Poon EK, Hutchins N, Thondapu V, Barlis P, Ooi A. 2017. Computational fluid dynamics study of common stent models inside idealised curved coronary arteries. Comput Methods in BiomeCh Biomed Eng. 20(6):671–681.

Chiastra C, Gallo D, Tasso P, Iannaccone F, Migliavacca F, Wentzel JJ, Morbiducci U. 2017. Healthy and diseased coronary bifurcation geometries influence near-wall and intravascular flow: a computational exploration of the hemodynamic risk. J Biomech. 58:79–88.

Gallo D, Steinman DA, Bijari PB, Morbiducci U. 2012. Helical flow in carotid bifurcation as surrogate marker of exposure to disturbed shear. J Biomech. 45(14): 2398–2404.

Gataulin YA, Zaitsev DK, Smirnov EM, Fedorova EA, Yukhnev AD. 2015. Weakly swirling flow in a model of blood vessel with stenosis: Numerical and experimental study. St Petersburg Polytechnical University Journal: Physics and Mathematics. 1(4):364–371.

Ha H, Choi W, Lee SJ. 2015. Beneficial fluid-dynamic features of pulsatile swirling flow in 45 end-to-side anastomosis. Med Eng Phy. 37(3):272–279.

Ha H, Choi W, Park H, Lee SJ. 2015. Effect of swirling blood flow on vortex formation at post-stenosis. Proc Inst Mech Eng H. 229(2):175–183.

Ha H, Hwang D, Choi W-R, Baek J, Lee SJ. 2014. Fluid-dynamic optimal design of helical vascular graft for stenotic disturbed flow. PloS One. 9(10):e111047.

Ha H, Lee S-J. 2013. Hemodynamic features and platelet aggregation in a stenosed microchannel. Microvascular Research. 90:96–105.

Ha H, Lee SJ. 2014. Effect of pulsatile swirling flow on stenosed arterial blood flow. Med Eng Phys. 36(9): 1106–1114.

Himburg HA, Grzybowski DM, Hazel AL, LaMack JA, Li X-M, Friedman MH. 2004. Spatial comparison between wall shear stress measures and porcine arterial endothelial permeability. Am J Physiol Heart Circ Physiol. 286(5):H1916–H1922.

Hoi Y, Wasserman BA, Xie YJ, Najjar SS, Ferruci L, Lakatta EG, Gerstenblith G, Steinman DA. 2010. Characterization of volumetric flow rate waveforms at the carotid bifurcations of older adults. Physiol Meas. 31(3):291.

Houston JG, Gandy SJ, Milne W, Dick JB, Belch JJ, Stonebridge PA. 2004. Spiral laminar flow in the abdominal aorta: a predictor of renal impairment deterioration in patients with renal artery stenosis?. Nephrol Dial Transplant. 19(7):1786–1791.

Huang Y, Teng Z, Sadat U, Graves MJ, Bennett MR, Gillard JH. 2014. The influence of computational strategy on prediction of mechanical stress in carotid atherosclerotic plaques: comparison of 2D structure-only, 3D structure-only, one-way and fully coupled fluid-structure interaction analyses. J Biomech. 47(6):1465–1471.

Hunt J, Hussain F. 1991. A note on velocity, vorticity and helicity of inviscid fluid elements. J Fluid Mech. 229(1): 569–587.

Jiménez JM, Davies PF. 2009. Hemodynamically driven stent strut design. Ann Biomed Eng. 37(8):1483–1494.

Kilner PJ, Yang GZ, Mohiaddin RH, Firmin DN, Longmore DB. 1993. Helical and retrograde secondary flow patterns in the aortic arch studied by three-directional magnetic

resonance velocity mapping. Circulation. 88(5 Pt 1): 2235–2247.
Kolář V. 2007. Vortex identification: new requirements and limitations. Int J Heat Fluid Flow. 28(4):638–652.
Ku DN, Giddens DP. 1983. Pulsatile flow in a model carotid bifurcation. Arteriosclerosis. 3:31–39.
Ku DN, Giddens DP, Zarins CK, Glagov S. 1985. Pulsatile flow and atherosclerosis in the human carotid bifurcation. Positive correlation between plaque location and low oscillating shear stress. Arteriosclerosis. 5:293–302.
Lantz J, Henriksson L, Persson A, Karlsson M, Ebbers T. 2016. Patient-specific simulation of cardiac blood flow from high-resolution computed tomography. J Biomech Eng. 138(12):121004.
Lee KE, Lee JS, Yoo JY. 2011. A numerical study on steady flow in helically sinuous vascular prostheses. Med Eng Phys. 33(1):38–46.
Lee S-W, Steinman DA. 2007. On the relative importance of rheology for image-based CFD models of the carotid bifurcation. J Biomech Eng. 129(2):273–278.
Liang H, Maxworthy T. 2005. An experimental investigation of swirling jets. J Fluid Mech. 525:115–159.
Linge F, Hye MA, Paul MC. 2014. Pulsatile spiral blood flow through arterial stenosis. Comput Methods Biomech Biomed Engin. 17(15):1727–1737.
Liu X, Sun A, Fan Y, Deng X. 2015. Physiological significance of helical flow in the arterial system and its potential clinical applications. Ann Biomed Eng. 43(1):3–15.
Ma P, Li X, Ku DN. 1997. Convective mass transfer at the carotid bifurcation. J Biomech. 30(6):565–571.
Morbiducci U, Ponzini R, Rizzo G, Cadioli M, Esposito A, De Cobelli F, Del Maschio A, Montevecchi FM, Redaelli A. 2009. In vivo quantification of helical blood flow in human aorta by time-resolved three-dimensional cine phase contrast magnetic resonance imaging. Ann Biomed Eng. 37(3):516.
Morbiducci U, Ponzini R, Rizzo G, Cadioli M, Esposito A, Montevecchi FM, Redaelli A. 2011. Mechanistic insight into the physiological relevance of helical blood flow in the human aorta: an in vivo study. Biomech Model Mechanobiol. 10(3):339–355.
Mukherjee D, Padilla J, Shadden SC. 2016. Numerical investigation of fluid–particle interactions for embolic stroke. Theor Comput Fluid Dyn. 30(1-2):23–39.
Paul MC, Larman A. 2009. Investigation of spiral blood flow in a model of arterial stenosis. Med Eng Phys. 31(9):1195–1203.
Perktold K, Resch M, Peter RO. 1991. Three-dimensional numerical analysis of pulsatile flow and wall shear stress in the carotid artery bifurcation. J Biomech. 24(6): 409–420.
Pinto S, Campos J. 2016. Numerical study of wall shear stress-based descriptors in the human left coronary artery. Comput Methods Biomech Biomed Eng. 19(13): 1443–1455.
Prashantha B, Anish S. 2018. Discrete-Phase modelling of an asymmetric stenosis artery under different womersley numbers. Arab J Sci Eng. 1:15.
Schulz UG, Rothwell PM. 2001. Major variation in carotid bifurcation anatomy: a possible risk factor for plaque development?. Stroke. 32(11):2522–2529.
Soulis JV, Lampri OP, Fytanidis DK, Giannoglou GD. Relative residence time and oscillatory shear index of non-Newtonian flow models in aorta. Proceedings of the Biomedical Engineering, 2011. 10th International Workshop on; 2011: IEEE.
Steinman DA, Poepping TL, Tambasco M, Rankin RN, Holdsworth DW. 2000. Flow patterns at the stenosed carotid bifurcation: effect of concentric versus eccentric stenosis. Ann Biomed Eng. 28(4):415–423.
Stonebridge P, Brophy C. 1991. Spiral laminar flow in arteries? Lancet. 338(8779):1360–1361.
Stonebridge P, Buckley C, Thompson A, Dick J. 2004. Non spiral and spiral (helical) flow patterns in stenoses: in vitro observations using spin and gradient echo magnetic resonance imaging (MRI) and computational fluid dynamic modeling. International Angiology. 23:276.
Sullivan TM, Zeller T, Nakamura M, Caro CG, Lichtenberg M. 2018. Swirling flow and wall shear: evaluating the biomimics 3d helical centerline stent for the femoropopliteal segment. Int J Vasc Med. 2018:10.
Sun A, Fan Y, Deng X. 2010. Numerical comparative study on the hemodynamic performance of a new helical graft with noncircular cross section and swirlgraft. Artificial Organs. 34(1):22–27.
Tan F, Soloperto G, Bashford S, Wood N, Thom S, Hughes A, Xu X. 2008. Analysis of flow disturbance in a stenosed carotid artery bifurcation using two-equation transitional and turbulence models. J Biomech Eng. 130(6):061008.
Van Canneyt K, Morbiducci U, Eloot S, De Santis G, Segers P, Verdonck P. 2013. A computational exploration of helical arterio-venous graft designs. J Biomech. 46(2): 345–353.
Varghese SS, Frankel SH, Fischer PF. 2007. Direct numerical simulation of stenotic flows. Part 1. Steady flow. J Fluid Mech. 582:253–280.
Varghese SS, Frankel SH, Fischer PF. 2008. Modeling transition to turbulence in eccentric stenotic flows. J Biomech Eng. 130(1):014503.
Wen J, Zheng T, Jiang W, Deng X, Fan Y. 2011. A comparative study of helical-type and traditional-type artery bypass grafts: numerical simulation. Asaio J. 57(5): 399–406.
WHO 2016. Hearts: technical package for cardiovascular disease management in primary health care. World health organisation ed.
Wong KKL, Cheung SCP, Yang W, Tu J. 2010. Numerical simulation and experimental validation of swirling flow in spiral vortex ventricular assist device. Int J Artif Organs. 33(12):856–867.
Zeller T, Gaines PA, Ansel GM, Caro CG. 2016. Helical centerline stent improves patency: two-year results from the randomized mimics trial. Circ: Cardiovasc Interv.9: e002930.
Zheng T, Wen J, Jiang W, Deng X, Fan Y. 2014. Numerical investigation of oxygen mass transfer in a helical-type artery bypass graft. Comput Methods Biomech Biomed Eng. 17(5):549–559.
Zovatto L, Pedrizzetti G. 2017. Fluid flow in a helical vessel in presence of a stenosis. Meccanica. 52(3):545–553.